Composites Part A 130 (2020) 105723

Contents lists available at ScienceDirect

Composites Part A

journal homepage: www.elsevier.com/locate/compositesa

Effects of resin distribution patterns on through-thickness air removal in vacuum-bag-only prepregs

Sarah G.K. Schechter*, Timotei Centea, Steven Nutt

Department of Chemical Engineering and Materials Science, University of Southern California, Los Angeles, CA 90089, USA

ARTICLE INFO

Keywords:
A. Prepreg
A. Polymer-matrix composites
B. Permeability
E. Out of autoclave processing

ABSTRACT

Prepregs with discontinuous resin patterns facilitate air removal and impart robustness to vacuum-bag-only processing of composites. However, optimal pattern characteristics have not yet been identified. A geometric model was developed to guide the fabrication of prepregs with various discontinuous patterns and laminates with different orientations and ply counts. The model was used to evaluate metrics related to gas transport: projected surface area exposed, sealed interfaces, and tortuosity. Statistical analysis revealed that single layer surface area exposed and ply count had the greatest effect on projected surface area exposed; orientation had the greatest effect on sealed interfaces and tortuosity. From these insights, prototype prepregs were fabricated to measure through-thickness permeability. Prepregs with a large percentage of sealed interfaces and high tortuosity exhibited lower permeability. The study demonstrated a methodology to differentiate/screen patterns for gas transport efficiency. The model can guide prepreg design and support robust production of composites via out-of-autoclave manufacturing.

1. Introduction

Prepregs processed via out-of-autoclave (OoA) vacuum-bag-only (VBO) methods offer an increasingly viable alternative to traditional autoclave manufacturing methods [1]. VBO prepregs alleviate problems associated with the autoclave, including high costs from acquiring and operating pressure vessels, limited throughput (i.e., production bottlenecks), and high resource use (e.g., energy, nitrogen gas). However, OoA/VBO processing is limited to 0.1 MPa (1 atm) of consolidation pressure, which is often insufficient to collapse porosity to acceptable levels. Consequently, if entrapped gases are not completely evacuated during early stages of processing, VBO-cured parts will exhibit porosity and diminished mechanical properties [2].

Conventional VBO prepregs are fabricated by pre-impregnating the fiber bed using a hot-melt process: pre-catalyzed resin is formed into a thin film on backing paper and pressed onto the fiber bed using rollers [3,4]. By design, the resulting prepreg includes dry, highly permeable gas evacuation pathways at the mid-plane of the ply. Combined with appropriate consumables, such as edge-breathing dams, these pathways can be sufficient to achieve low defect levels (i.e., porosity) within cured parts [5]. However, in laminates fabricated from conventional VBO prepregs, sub-optimal conditions such as inadequate vacuum, high levels of absorbed moisture in the resin, or part geometries that prevent in-plane air removal can lead to unacceptable void levels [6,7].

1.1. Background

Past work has shown that *discontinuous* resin films increase the capacity for air evacuation in the *z*-direction (transverse) by creating additional egress pathways, and can virtually eliminate porosity caused by entrapped gases and low-pressure VBO consolidation [8–10]. For example, Roman showed that the resultant cured composite parts using prepreg with discontinuous resin film exhibited near-zero internal porosity [8]. In related work, Grunenfelder et al. showed that, even under non-ideal manufacturing conditions, a discontinuous prepreg format (denoted USCpreg) produced near-zero internal porosity and no surface defects [9]. In contrast, under identical manufacturing conditions, prepreg with continuous resin resulted in high porosity levels. Grunenfelder's work demonstrated that the USCpreg format was more robust than conventional VBO prepregs. Finally, Tavares et al. measured the through-thickness air permeability at room temperature and processing conditions of a commercial semipreg ("Zpreg") and an equivalent unidirectional prepreg constructed with continuous resin [10]. Results showed that the permeability of the semipreg was three orders of magnitude greater than the continuous film prepreg before and during the cure cycle, owing to a network of dry interconnected pore spaces. Their work showed that the initial overall dry space in prepreg prior to cure increased when the resin distribution was discontinuous. Nevertheless, these works together demonstrated the

* Corresponding author.
E-mail address: sarahgka@usc.edu (S.G.K. Schechter).

https://doi.org/10.1016/j.compositesa.2019.105723
Received 16 April 2019; Received in revised form 4 December 2019; Accepted 6 December 2019
Available online 12 December 2019
1359-835X/

increased robustness of prepreg with discontinuous resin. This beneficial effect can be attributed to the much shorter distance for air evacuation in the through-thickness direction as compared to the in-plane direction. However, methods of production allowing for the creation of arbitrary patterns on a chosen fiber bed were not identified or disclosed.

Previously, we demonstrated a simple technique to create discontinuous resin patterns via polymer film dewetting on a substrate [11]. Resin film was perforated on silicone-coated backing paper (i.e., the substrate) to create an array of nucleation sites. The film was then heated, which caused resin to recede from the perforated sites, nucleating dewetted openings. The resin recession was driven by the surface tension between the low surface energy substrate (the silicone-coated backing paper) and the resin [12–15]. Finally, the dewetted resin was transferred onto the fiber bed by pressing briefly. This technique can be used to create a variety of resin patterns, including stripes, grids, and islands. In addition, the patterned resin films created with this technique can be applied to any dry fiber bed.

1.2. Objectives

Polymer film dewetting allows for the creation of resin distribution patterns with varying shapes and sizes. However, this capability substantially enlarges the design space for the prepeg format. The optimal pattern for efficient air evacuation has not been identified yet, nor is it obvious. In addition, the relationships between pattern characteristics, laminate design (i.e., stacking orientation, ply count), and prepreg properties with regards to z-direction air evacuation are unclear. Because of the extensive design space possible for VBO prepregs featuring these new formats, experimental screening based on prepreg production, laminate layup, and permeability testing will be arduous, time-consuming, and ineffective in highlighting governing trends. Thus, the present work focused on developing a method to (1) screen (evaluate and differentiate) between discontinuous resin patterns without excessive experimentation or set-up time, and (2) identify prepreg characteristics that likely favor rapid air evacuation in the transverse direction in the initial state (i.e., at room temperature, before significant flow-compaction has occurred).

These objectives were accomplished by developing a program (in MATLAB) to generate geometric models of the prepreg (in 2D) and of an arbitrary laminate (in 3D). Methods were implemented for measuring several attributes from these models: projected surface area exposed of stacked prepreg, sealed interfaces, and tortuosity of the air evacuation pathway. Subsequently, a factorial design study was conducted to determine the effect of pattern factors on each of these attributes. The factorial design was analyzed using n-way ANOVA and multi-comparison tests. The results from the multi-comparison tests were used to select laminates for experimental validation. Finally, the effective air permeability at room temperature of these laminates was tested. The study effectively outlines a methodology that can readily discriminate between prepreg designs and allow for the rapid selection of prepregs that efficiently evacuate air.

2. Modeling

2.1. Model development

The primary goal of modeling was to create a method for rapidly screening prepreg configurations (and resulting laminates) with respect to initial capacity for transverse air evacuation at room temperature. Thus, explicitly modeling resin flow and fiber bed compaction for an arbitrary discontinuous prepreg laminate was excluded from the scope of this first effort. The capacity for gas flow within complex-shaped porous media can be estimated using different approaches, including geometric analysis (employed here), analytical models of flow in porous media, and computational simulations. Analytical models capture and express the underlying physics, and such models have been used to generate process maps to guide material or process development [16–19]. Computational models allow detailed, often multi-physics analysis of physical phenomena within complex domains [20]. However, both methods must be configured and solved for a specific domain geometry. While parameterization of scales is possible, neither option is inherently well suited to broad, rapid screening of arbitrary prepreg and laminate patterns. For these reasons, this study focused on investigating the viability of a geometric model that is simple to implement (i.e., parametric) and execute, and that can reduce a large design space to a small subset of potential solutions, which can be evaluated experimentally.

The model developed here relied on simplifying assumptions. Prior work has shown that gas transport occurs much faster through dry regions (i.e., unsaturated fiber reinforcements) than through saturated regions [9,10,21]. Hence, the model was based on the premise that gas evacuation capacity is primarily governed by the characteristics (i.e., size and connectivity) of the dry pore network, rather than by bubble migration through resin. Hence, void growth and transport within the fluid domain were not modeled. Previous studies have also indicated that, following initial compaction, the microstructure of partially-impregnated prepregs does not evolve substantially under room-temperature vacuum compaction [22,23]. For this reason, the model utilized a rigid geometric framework, without simulating compaction. In addition, the thickness of a resin layer and a fiber layer were arbitrarily defined and remained constant across prepreg designs. However, in actuality, the thickness of the resin layer would increase with a decrease in resin feature dimensions.

2.2. Parametric study

2.2.1. Methods

Prepregs are generally produced by placing a continuous layer of resin on either or both side(s) of a fiber bed [Fig. 1a]. Usually, in OoA prepregs, the fiber bed is partially impregnated by the resin, where the dry space allows for in-plane evacuation of air via the ply mid-plane. In OoA prepreg formats that feature discontinuous resin, surface openings allow for additional air evacuation in the transverse direction [Fig. 1b]. A laminate is constructed by stacking plies of such prepreg. The placement of the resin on the fiber bed and the plies of prepreg for a laminate are random (i.e., no intentional alignment of features). The space between the resin layers of the stacked prepregs is an interface in which air can be readily entrapped. In addition, with discontinuous resin, this interface can either be sealed, if surface openings are too small, or not sealed, allowing for an interconnected evacuation pathway in the transverse direction.

The code was written to create patterns that replicate those that have been created by the polymer film dewetting technique [11]. These patterns included stripes, islands, and grids [Fig. 2a]. To create these patterns, rectangles in 2D coordinates were created using a four-element vector of the form [x y w h]. The x and y elements determine the location, and the w and h elements determine the size. Curvature was also specified, where a value of 0 results in no curvature, and a value of 1 results in maximum curvature. For stripes, the curvature of the rectangle was set to 0, whereas for islands and grids, the curvature was set to 1. The islands and grid patterns were programmed to be mutually reciprocal by computing the complement of the image. In addition, the images were cropped to the same size to eliminate any automatically created borders. Fig. 2b shows examples of a single resin ply created by this method for each of the three pattern types studied. Black regions represent void space (defined as a pixel intensity of 0) and white regions represent resin (a value of 1).

The code was designed so that the laminate was symmetrical about the midpoint [Table 1]. Thus, the resin layers that make up the interface at the midpoint were oriented in the same direction. Each resin layer was randomly translated in the x- and y-directions by generating a

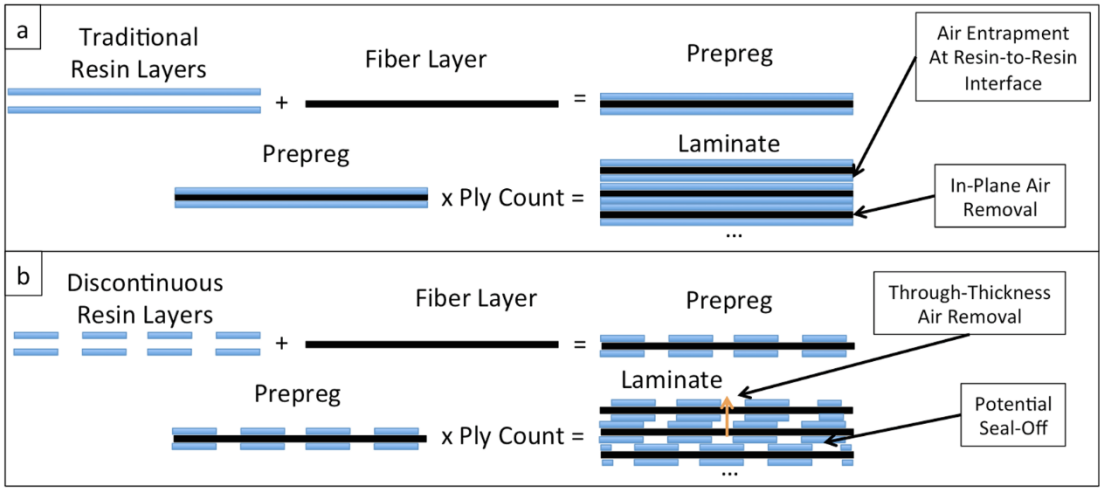

Fig. 1. (a) The traditional manufacture of prepreg and laminates with continuous resin, illustrating air entrapment at the resin-to-resin interface and the mechanism of air removal in the mid-plane. (b) The fabrication of prepreg and laminates with a discontinuous resin distribution, illustrating air removal in the through-thickness direction and the potential for seal-off between resin layers (due to large resin feature dimensions and random placement during stacking).

single uniformly distributed random number in the interval (0,1). This random number was multiplied by the phase, which was the sum of the resin distance and the dry space distance, then added to the location elements in the four-element vector.

Three key output attributes were defined to generate a broad description of the air evacuation capacity of a laminate constructed with discontinuous resin patterns: (a) the two-dimensional projected exposed surface area (%) of a laminate, (b) the percentage of sealed interfaces in a laminate (relative to the total number of inter-ply regions), and (c) the tortuosity of the dry pore network pathways in the laminate. The 2D projection of the exposed surface area (%) described the presence and amount of direct (unoccluded) transverse-oriented pathways. However, even with zero projected surface area exposed, gases can move in the through-thickness direction by migrating laterally through the dry fibers. Hence, the percentage of sealed interfaces described the number of occlusions in the modeled pore network for flow in the transverse direction. A sealed interface is created when the resin films on adjacent prepreg plies are stacked such that film openings are sealed off, effectively generating a continuous film. In such cases, continuous through-thickness evacuation pathways will not exist from laminate bottom to top. Finally, tortuosity described the distance gas would have to travel within in the laminate to escape (assuming no

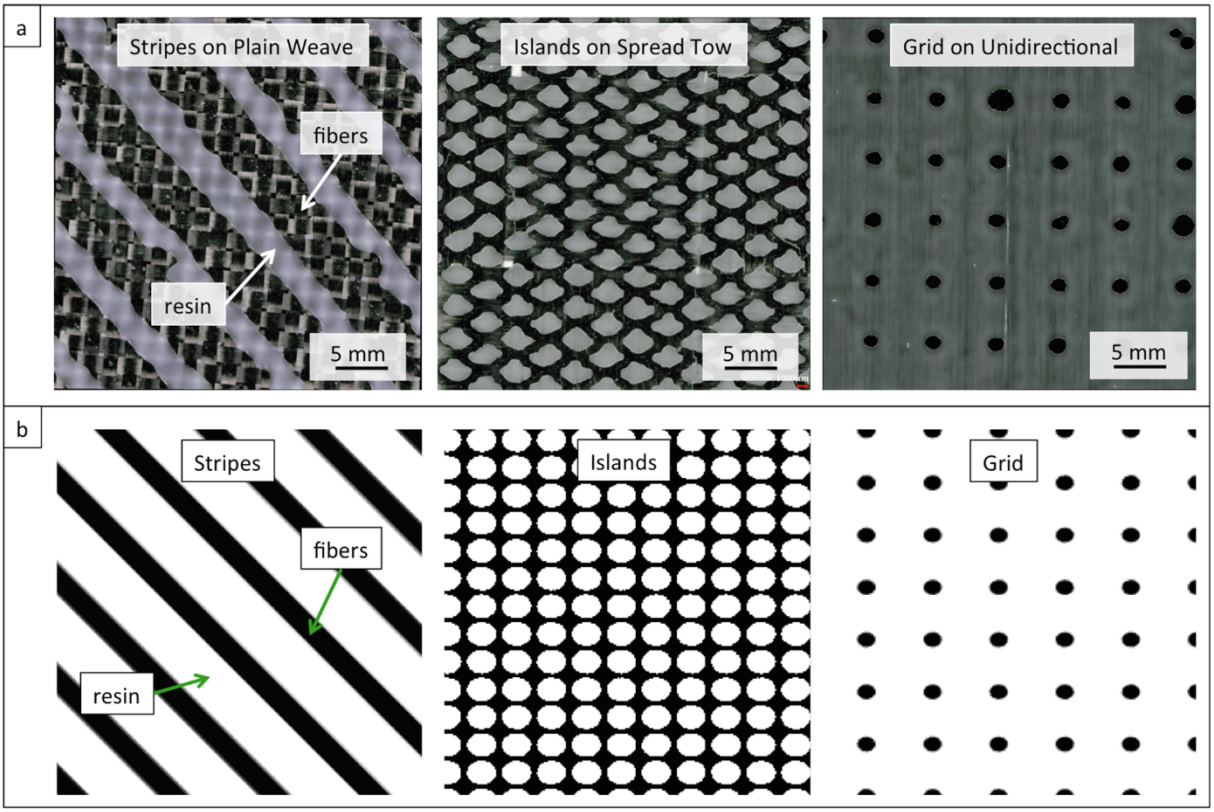

Fig. 2. (a) Examples of the discontinuous resin patterns created via the polymer film dewetting technique. (b) Examples of the discontinuous resin patterns coded in MATLAB.

Table 1
List of the stacking sequences at 4, 8, and 16 plies implemented into the code.

[0/0]n	
4 Ply	[0, 0, 0, 0] x1
8 Ply	[0, 0, 0, 0] x2
16 Ply	[0, 0, 0, 0] x4
$[0/90]_n$	
4 Ply	0, 90, 90, 0
8 Ply	0, 90, 0, 90, 90, 0, 90, 0
16 Ply	0, 90, 0, 90, 0, 90, 0, 90, 90, 0, 90, 0, 90, 0, 90, 0
$[0/90/\pm 45]_n$	
4 Ply	0, 90, +45, −45
8 Ply	0, 90, +45, −45, −45, +45, 90, 0
16 Ply	0, 90, +45, −45, 0, 90, +45, −45, −45, +45, 90, 0, −45, +45, 90, 0

sealed interfaces). If the laminate contained a sealed interface, then the laminate would not have a tortuous path available for air evacuation. Large tortuosity values were expected to reduce the momentum of gas flow, thereby reducing permeability, even in the absence of sealed interfaces. The input and output variables are outlined in Table 2.

Each parameter computation was iterated 25 times to achieve an average value. When prepreg and laminates are manufactured, the resin layers are randomly placed on the fiber bed, and thus the iterations would compensate for the randomness in making prepregs and laminates. The parameters were calculated for 4, 8, and 16 plies (i.e., 8, 16, and 32 resin layers or 3, 7, and 15 interfaces). Three orientations were programmed for computation: $[0/0]_n$, $[0/90]_n$, and $[0/90/\pm 45]_n$ (i.e., quasi-isotropic).

The code for the three parameters is illustrated in a flowchart in Fig. 3. For calculations of projected surface area exposed (%), the laminates (or "stacks") were created by matrix addition of the appropriate number of resin layers according to the target ply count. The surface area exposed (%), A_{SE}, then was calculated using the following equation:

$$A_{SE} = \frac{No.\ \ of\ \ Zero\ \ Elements}{Total\ \ No.\ \ of\ \ Elements} \times 100\% \tag{1}$$

For sealed interfaces (%) calculations, an interface was created by the matrix addition of two resin layers. The number of interfaces created for each laminate was 3 for 4 plies, 7 for 8 plies, and 15 for 16 plies. The exposed surface area (%) of the interface was calculated from Eq. (1). A threshold value of 0.1% was employed, where, if the surface area exposed (%) was less than 0.1%, then the interface was considered sealed. Otherwise, the interface was not sealed. The percentage of sealed interfaces was calculated by:

$$Sealed\ \ Interfaces\ \ (\%) = \frac{Average\ \ No.\ \ of\ \ Sealed\ \ Interfaces}{Total\ \ No.\ \ of\ \ Interfaces} \times 100\% \tag{2}$$

For tortuosity calculations, 3D objects were created to represent the laminates fabricated with discontinuous resin. The dry fiber layers between the resin layers were modeled as dry space by creating matrices of all zeroes. The "fiber layers" were not rotated nor translated. The "resin layers" were constructed just as before, in that the layers were rotated and randomly translated (in plane). Each fiber layer was four pixels thick, and each resin layer was two pixels thick. Examples of how the 3D objects were rendered are shown in Fig. 4. Next, the tortuosity of the transverse air evacuation pathways was calculated using the TORT3D.m program developed by Al-Raoush et al. [24]. The code read a segmented image and determined all possible tortuous pathways required to compute tortuosity. The algorithm conducted a guided search for the connected path in the void space of the image, utilizing the medial surface of the void space. The average of all connected pathways in that direction was used to compute tortuosity. Geometric tortuosity, τ_g, was defined as:

$$\tau_g = \frac{\langle L_g \rangle}{L_s} \tag{3}$$

where $\langle L_g \rangle$ is the average length of true paths through the porous media, and L_s is the length of the straight-line path across the porous media in the direction of flow. The tortuosity value, τ, acquired from the code was defined as:

$$\tau = \frac{\frac{\sum_{i=1}^{n} l_{p_i}}{n}}{l_s} \tag{4}$$

where l_p is the given path through the void space that connects the boundary of the images in the direction of flow, l_s is the corresponding straight line, and n is the number of paths. If the 3D object contained a sealed interface, the program returned a tortuosity value of "NaN," meaning the program was unable to compute a value.

2.2.2. Results

Single layer A_{SE}: The exposed surface area (%) [Eq. (1)] of a single discontinuous resin film was determined for all three pattern types for resin widths or diameters specified between 1 and 20 pixels, and dry space distance specified between 1 and 20 pixels [Fig. 5]. The graphs in Fig. 5a-c show the limitations of the amount of initial (or single layer) surface area exposed. The stripes pattern [Fig. 5a] yielded the largest range of exposed surface area (%), with values from 10% to 90%. However, an upper limit of 90% appeared to exist for the stripes pattern. For the islands pattern [Fig. 5b], no upper limit appeared to exist, but a lower limit of 15% did manifest. As for the grid pattern [Fig. 5c], no lower limit existed, but an upper limit of 65% did exist. With all three constraints considered, the range of surface area exposed (%) that could be used for comparison between the three patterns was 15–65%.

Projected A_{SE}: The projected surface area exposed (%) was calculated

Table 2
List of input and output variables of the developed code.

Input Variables	
Pattern Type	Specify the type of pattern (here, stripes, islands, or grid)
Resin Distance and Dry Space Distance	Specify the feature dimension sizes of both the resin and the dry space (here, the range of values used were from 1 to 20)
Orientation	Specify the orientation of the stacking sequence (here, $[0/0]_n$, $[0/90]_n$, $[0/90/\pm 45]_n$)
Ply Count	Specify the number of plies (here, 4, 8, or 16)
Output Variables	
Average A_{SE}	Calculate the average surface area exposed (%) from all the iterations
Average No. of Sealed Interfaces	Calculate the average number of sealed interfaces from all the iterations
Percent Sealed Interfaces	Calculate percentage of interfaces that are sealed using Eq. (2)
Average Tortuosity	Calculate the average tortuosity value from all the iterations

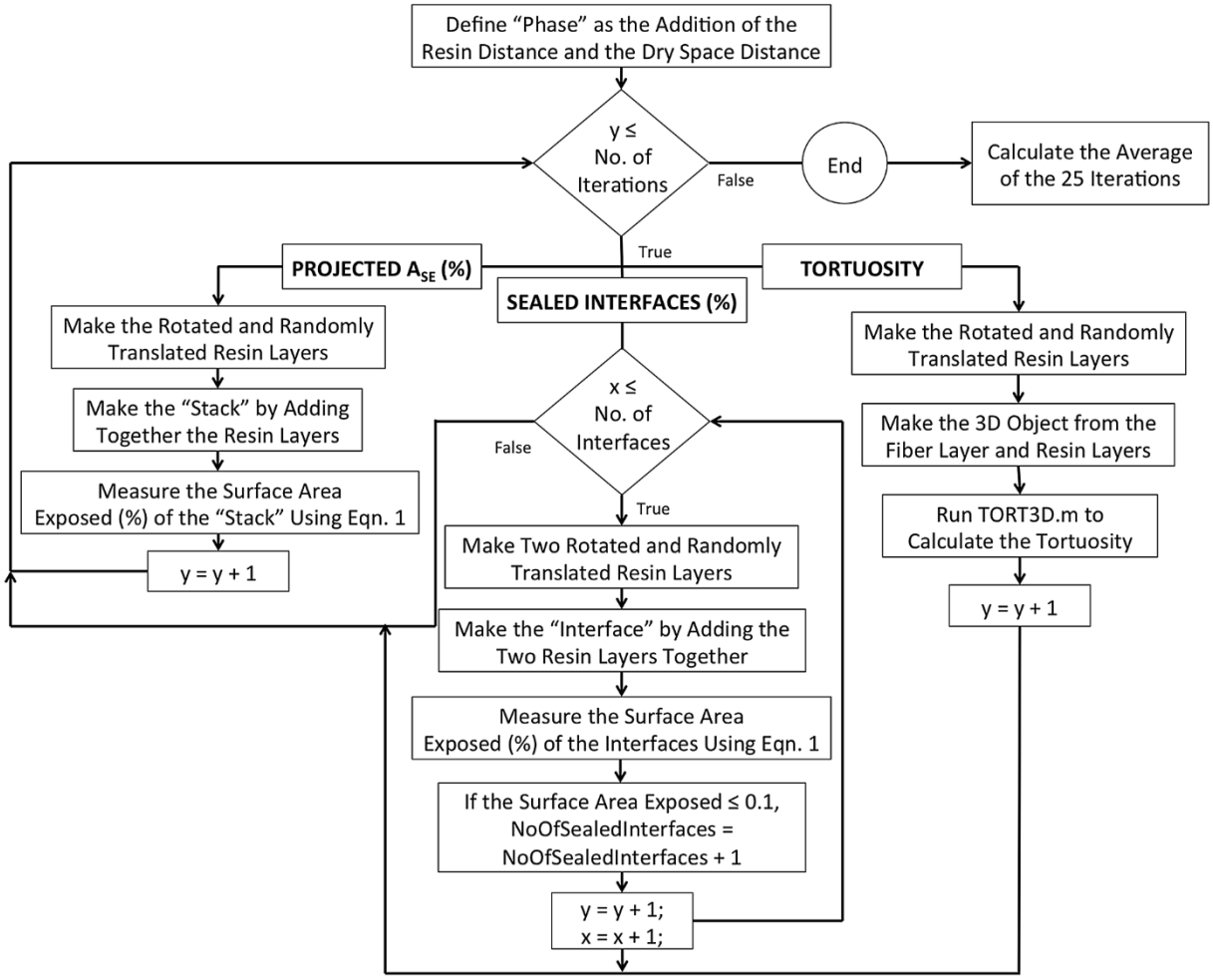

Fig. 3. A flow chart of the developed algorithms to create the resin layers, resin interfaces, and 3D objects to compute the surface area exposed (%) of the "stacked" images, sealed interfaces within the specified ply count, and tortuosity, respectively.

as each resin layer was added to the stack. These computations were performed for single-layer surface area exposed values of 30% and 60%. Fig. 6a compares the projected surface area exposed (%) of the three patterns (stripes, islands, and grid). Provided the single layer surface area exposed (%) value was the same, the decrease in projected surface area exposed (%) was the same across the pattern types. Fig. 6b compares the projected exposed surface area (%) for the stripes pattern oriented in $[0/0]_n$, $[0/90]_n$, and $[0/90/\pm45]_n$. Orientation had a negligible effect on the behavior of how the projected surface area exposed (%) decreased. These graphs also show the point where the projected surface area exposed (%) approached zero. For 30% single layer surface area exposed, the projected surface area exposed (%) was nearly zero after just 2 plies (or 4 resin layers). For 60% single layer surface area exposed, the projected surface area exposed (%) was nearly zero after 5 plies are laid down (or 10 resin layers).

Sealed interfaces: The percentage of sealed interfaces (%) was calculated for 16-ply laminates with values of single resin layer surface area exposed between 7.5% and 60%. Fig. 7a compares the sealed interfaces across the three patterns (stripes, islands, and grid) with an orientation of $[0/0]_n$. The striped pattern resulted in substantial amounts of sealed interfaces (10.1 − 87.2%) at values of single layer surface area exposed (%) less than 60%. The grid pattern also produced substantial amounts of sealed interfaces (9.9–61.1%) when the single layer surface area exposed (%) was less than 45%. On the other hand, islands only yielded sealed interfaces when the single layer surface area exposed was less than 30%. However, an islands design with a single layer surface area exposed of 7.5% could not be obtained, so the sealed interfaces could not be determined at this value.

Fig. 7b compares the number of sealed interfaces for 16-ply laminates laid up with stripes in each of the three orientations ($[0/0]_n$, $[0/90]_n$, and $[0/90/\pm45]_n$). Intuitively, stripes would appear to be the most sensitive of the three patterns to orientation. Here, the data shows that $[0/90]_n$ and $[0/90/\pm45]_n$ laminates behaved identically, where the proportion of sealed interfaces was markedly less than for $[0/0]_n$. Intuitively, laminates produced with resin stripes oriented in either $[0/90]_n$ and $[0/90/\pm45]_n$ should not exhibit any sealed interfaces because the stripes were orthogonal. However, at the midpoint, the stacking was symmetric (the stripes were parallel), which could cause a sealed interface in certain cases of the randomly oriented set [Table 1].

Tortuosity: Tortuosity (a unitless quantity) was calculated for 16-ply laminates. Fig. 7c compares these laminates stacked in the orientation of $[0/90]_n$ for stripes, islands, and grid. On average, the stripes had greater tortuosity than either the island or grid patterns. The island and grid patterns behaved similarly with high single layer surface areas exposed. Fig. 7d compares the 16 ply stripes laminates oriented in $[0/0]_n$, $[0/90]_n$, and $[0/90/\pm45]_n$. The $[0/90]_n$ laminate on average had a smaller tortuosity. However, the $[0/90/\pm45]_n$ laminate resulted in unusually high tortuosity. The high tortuosity can be attributed to the fact that each ply of a laminate produced with a quasi-isotropic stacking orientation was oriented in a different direction. These different orientations would result in more indirect and convoluted pathways than a simpler orientation like $[0/0]_n$ and $[0/90]_n$.

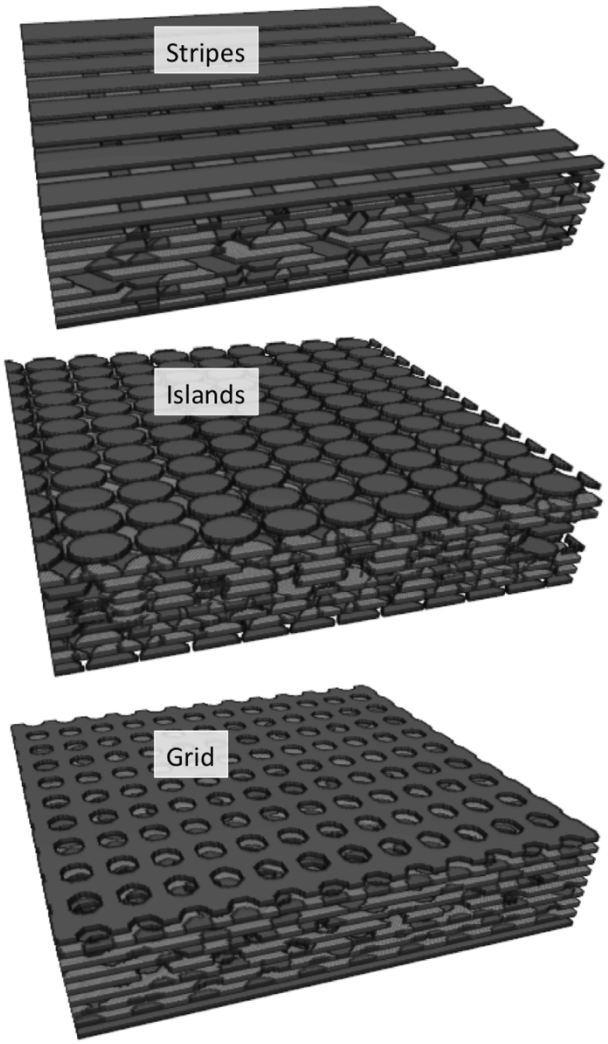

Fig. 4. Examples of the 3D objects coded in MATLAB to represent a laminate created with discontinuous resin patterns. Each object was 8 plies, quasi-isotropic, and 30% single layer surface area exposed.

2.3. Statistical analysis

Full factorial experiment: A full factorial experiment consists of two or more factors such as, in this case, pattern type and ply count. Each factor has discrete values or levels, such as, here, 4, 8 and 16 plies for ply count. The resulting values from the full factorial experiment take on all possible combinations of these levels across all such factors [25,26]. Such an experiment allows evaluation of the effects of each factor on the dependent variables, as well as the importance of interactions between factors. Here, each experiment (for each dependent variable) was denoted as a 3^4 factorial, which identifies the number of factors (4), the number of levels each factor has (3), and the number of experimental conditions in the design ($3^4 = 81$). Also, three dependent variables (projected surface area exposed, sealed interfaces, and tortuosity) were being calculated. Therefore, the total number of calculations was 243 (3×81). The number of physical experiments that would be required to perform such a screening instead (with 25 iterations of each experiment) demonstrates the utility of the geometric model, which would be much faster to execute. As listed in Table 3, the four factors (with the three levels) studied were pattern type (stripes, islands, grid), single layer surface area exposed (30%, 45%, 60%), ply count (4, 8, 16), and stacking orientation ($[0/0]_n$, $[0/90]_n$, $[0/90/\pm 45]_n$).

Analysis of variance (ANOVA): The factorial experiment responses were analyzed using Analysis of Variance (ANOVA). ANOVA is a collection of statistical models, and their associated estimation procedure (such as the variation among and between groups) is used to analyze the differences among group means in a sample [27,28]. In its simplest form, ANOVA provides a statistical test of whether the population means of several groups were equal, and therefore generalizes the *t*-test to more than two groups.

A test result (calculated from the null hypothesis and the sample) was treated as statistically significant if it was deemed unlikely to have occurred by chance, assuming the truth of the null hypothesis. A statistically significant result, i.e., when a probability (p-value) was less than a pre-specified threshold (here, $p \leq 0.05$), justified the rejection of the null hypothesis. The null hypothesis was that all groups were random samples from the same population. Rejecting the null hypothesis signified that the difference in observed effects between groups was unlikely to be because of random chance.

Initially, each experiment was performed using a 4-way ANOVA. However, terms often would have missing p-values (represented as "NaN"), indicating missing factor combinations and/or that the model had higher-order terms. Thus, a 3-way ANOVA was performed instead, which allowed for the identification of statistically insignificant terms. These terms were then omitted, where their effects were pooled into the error term. The *n*-way ANOVA was then performed again without the statistically insignificant terms. The ANOVA results for each response (dependent) variable are presented in Table 4.

For surface area exposed, the *p*-value was less than 0.05 (i.e., statistically significant) for only three of the factors – single layer surface area exposed, ply count, and orientation. This result signified that the projected surface area exposed (%) was insensitive to the pattern type. Comparing the *F*-values, the largest *F*-values for the projected surface area exposed (%) response variable was for ply count and single ply surface area exposed (%), which indicated that these two variables were the most influential on projected surface area exposed. The *F*-value is defined as

$$F = \frac{variation\ \ between\ \ sample\ \ means}{variation\ \ within\ \ the\ \ samples} \tag{5}$$

where the null hypothesis was that these two variance values were roughly equal (*F*-value = 1). Therefore, the larger the *F*-value, the greater the relative variance among the group, and thus, the greater the dependence of the dependent variable. The *p*-value indicates the probability of obtaining an *F*-value as extreme or more extreme than the one observed under the assumption that the null hypothesis was true.

For sealed interfaces (%), the ANOVA results indicated that all factors except ply count were significant, whereas for tortuosity, all factors were significant. Therefore, the number of plies of prepreg in a laminate had no effect on the percentage of sealed interfaces (i.e., not affected by scale), but ply count did affect tortuosity. The largest *F*-value for both the sealed interfaces and for tortuosity was the stacking orientation. The significance of the orientation may have been heavily skewed by its effect on the stripes pattern, which was the most sensitive to orientation.

Multiple comparison tests. Multiple comparison tests were performed to determine which groups of factors yielded statistically significant differences. To preserve clarity, the resulting interactive graphs of the estimates and comparison intervals were omitted. On the interactive graphs, each group mean was represented by a symbol, where a line extending out from the symbol represents the interval. Two group means were significantly different if their intervals were disjointed; they were not significantly different if their intervals overlapped. Any group can be selected and the graph will highlight all other groups that were significantly different.

For the 2D projected surface area exposed (%), the pattern type was determined to be insignificant, so the results were pooled together without regard to pattern type. The group with the largest mean (and being significantly different from the rest) was the 4-ply laminates made with 60% single layer surface area exposed and oriented $[0/0]_n$. The next two largest (significantly different) means, in order, were the same 4 ply laminates with 60% single resin surface area exposed, but

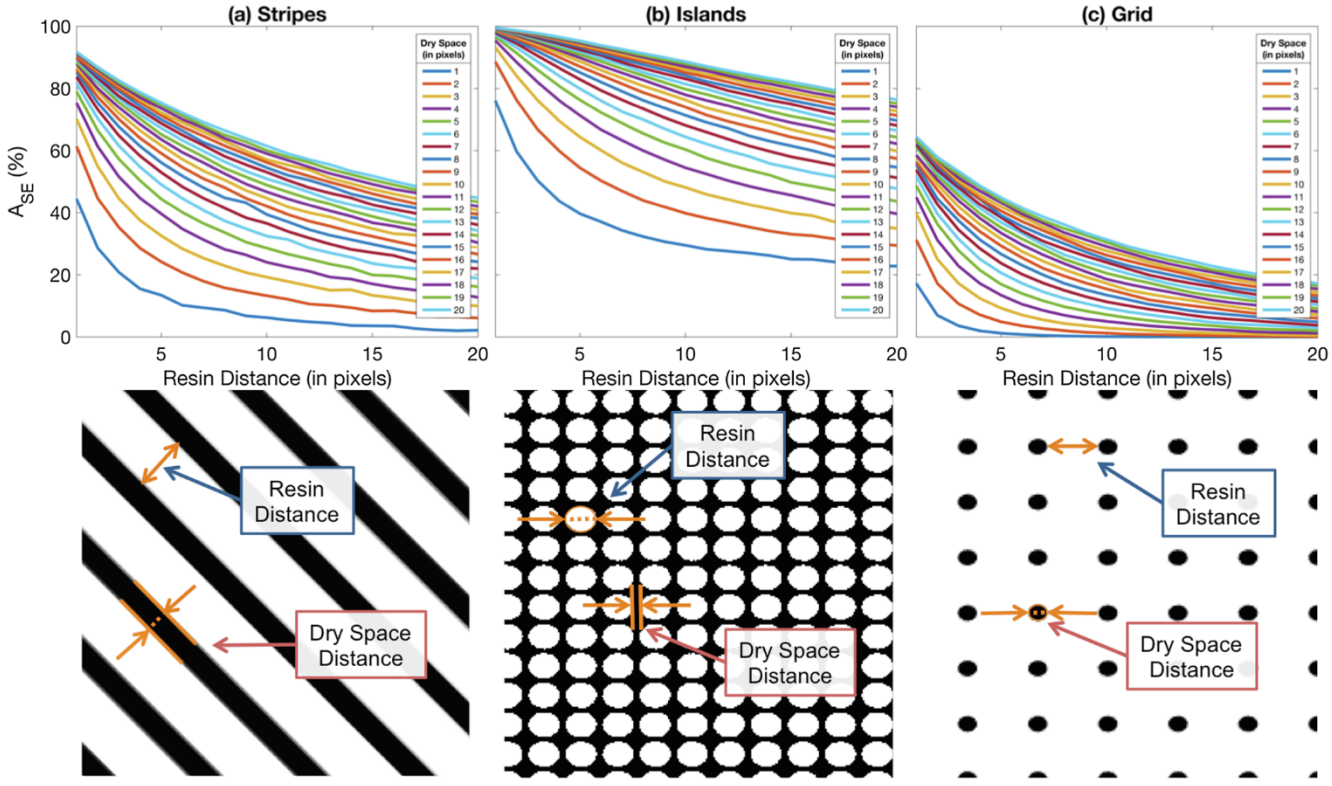

Fig. 5. Surface area exposed (%) for a single resin layer for each of the studied patterns [(a) stripes, (b) islands, (c) grid] with the specified range of resin and dry space distances of 1 to 20 pixels. Diagrams of the definition of the variables "Resin Distance" and "Dry Space Distance" are below each graph.

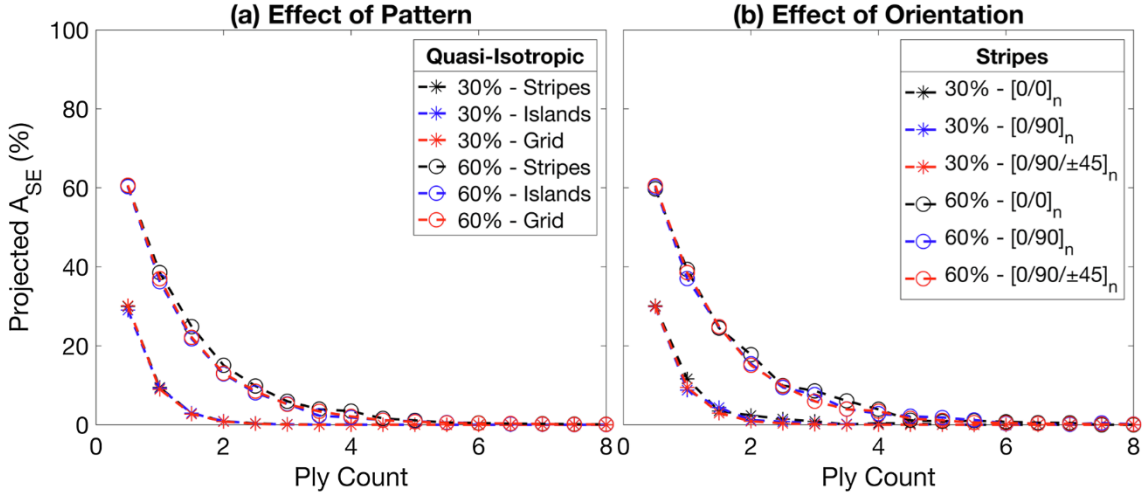

Fig. 6. Selected results of the projected surface area exposed (%) [(a) Quasi-Isotropic (b) Stripes] as ply count increases from the code developed.

oriented $[0/90]_n$ and $[0/90/\pm45]_n$. These conditions identified prepreg designs with the highest quantity of uninhibited air evacuation pathways in comparison to the other conditions tested (i.e. 4 plies, 60% A_{SE}, $[0/0]_n$). However, all three conditions were for 4-ply laminates, indicating that uninhibited air evacuation pathways did not exist for larger ply counts.

For sealed interfaces and tortuosity, ply count was ignored, because it was insignificant from the *n*-way ANOVA results. For sealed interfaces, three laminates exhibited the largest (significantly different) means, where all three were oriented $[0/0]_n$. Two of the laminates were stripes with 30% or 45% surface areas exposed, while the third laminate was a grid with 30% surface area exposed. These results indicated prepreg designs that would result in large amounts of sealed interfaces (i.e. stripes, 30% or 45% A_{SE}, $[0/0]_n$ and grid, 30% A_{SE}, $[0/0]_n$). For tortuosity, the largest mean was associated with the striped pattern with 30% surface area exposed and stacked in a $[0/90/\pm45]_n$ orientation. These results indicated a prepreg design that would result in high tortuosity (i.e., stripes, 30% A_{SE}, quasi-isotropic stacking). These multi-comparison results will be demonstrated in experimental verification testing, described next.

3. Experiments

Experiments were performed to (1) verify if geometric modeling can discriminate between prepregs with high and low room-temperature through-thickness gas permeability, and (2) determine which output attribute(s) most closely correlated to effective permeability and porosity in cured laminates.

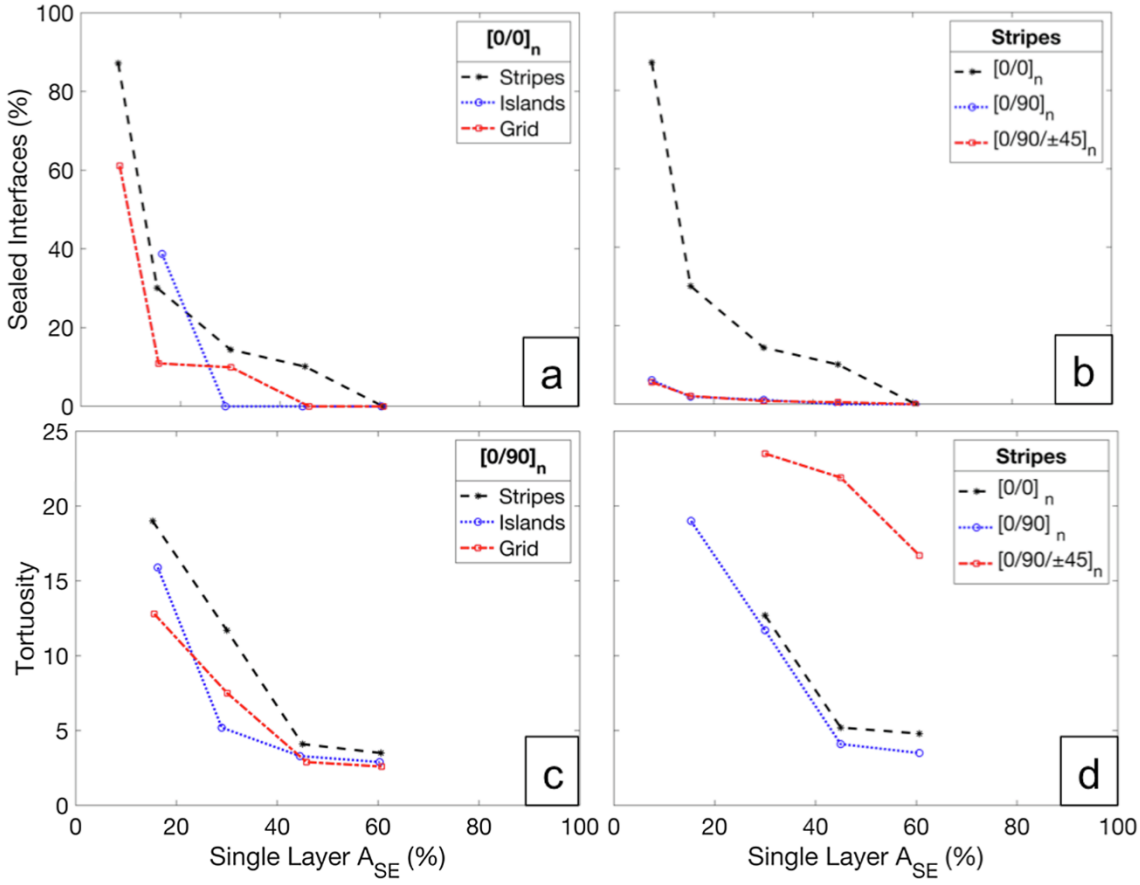

Fig. 7. Selected results of sealed interfaces (%) [(a) $[0/0]_n$ (b) Stripes] and tortuosity [(c) $[0/90]_n$ (d) Stripes] computations from the code developed for 16 ply laminates.

Table 3
List of factors and levels for the factorial design.

Factors	Levels
Pattern	Stripes, Islands, Grid
Single Layer Surface Area Exposed (%)	30, 45, 60
Ply Count	4, 8, 16
Stacking Orientation	$[0/0]_n$, $[0/90]_n$, $[0/90/\pm 45]_n$

3.1. Materials

A unidirectional (UD) non-crimp carbon fiber bed (Fibre Glast Development Corporation, Ohio, USA) and a toughened epoxy resin (PMT-F4, Patz Materials & Technology, California, USA) were selected for testing. The epoxy resin was designed for vacuum bag curing and featured medium-to-dry tack. The fabric weight was 305 g/m^2 (gsm), and the thickness was 0.36 mm. A binder of polyester fill threads stitched in one direction held the UD fibers in place. The tape exhibited negligible crimp, except around the binder threads. For the permeability tests, the resin film weighed 152 gsm, yielding prepreg with a resin content of 50% by weight, which was much larger than standard UD prepreg (i.e., 33%). Thick resin was used to ensure that the dewetting process yielded features that were close to the model image. The resin, at thinner thicknesses, occasionally dewetted at surface imperfections such as tears or depressions. For porosity measurements, prepregs were fabricated from two thicknesses of resin film – either 152 gsm or 76 gsm. The 152 gsm film was also used in permeability measurements, while the 76 gsm film was selected to match typical commercial prepregs. The 76 gsm film yielded prepreg with a resin content of 33%. The standard cure cycle included a ramp of 1.5 °C per min,

Table 4
Summary of the n-way ANOVA results for (a) the Projected Surface Area Exposed (%), (b) Sealed Interfaces (%), and (c) Tortuosity calculations.

Variable	F	Prob > F
Projected A_{SE} (%)		
Single Layer A_{SE} (%)	478.8	4.4E-35
Ply Count	493.5	2.0E-35
Orientation	32.7	4.9E-10
Single Layer A_{SE} (%) × Ply Count	404.9	1.5E-39
Single Layer A_{SE} (%) × Orientation	29.1	6.7E-13
Ply Count × Orientation	23.4	3.0E-11
Single Layer A_{SE} (%) × Ply Count × Orientation	20.3	9.3E-14
Sealed Interfaces (%)		
Pattern	28.6	3.4E-09
Single Layer A_{SE} (%)	45.8	2.3E-12
Orientation	61.9	1.1E-14
Pattern × Single Layer A_{SE} (%)	15.1	2.4E-08
Pattern × Orientation	17.4	3.1E-09
Single Layer A_{SE} (%) × Orientation	25.0	9.6E-12
Pattern × Single Layer A_{SE} (%) × Orientation	11.3	3.1E-09
Tortuosity		
Pattern	283.1	0
Single Layer A_{SE} (%)	264.8	0
Ply Count	20.7	0
Orientation	472.3	0
Pattern × Single Layer A_{SE} (%)	27.2	0
Pattern × Ply Count	14.8	0
Pattern × Orientation	152.9	0
Single Layer A_{SE} (%) × Ply Count	7.6	2.00E-04
Single Layer A_{SE} (%) × Orientation	31.7	0
Ply Count × Orientation	13.8	0
Pattern × Single Layer A_{SE} (%) × Orientation	8.7	0
Pattern × Ply Count × Orientation	2.9	1.50E-02

followed by a two-hour dwell at 121 °C.

Dewetting was performed as described previously [11]. To facilitate dewetting, nucleation sites were introduced using a box cutter. The dewetting process was carried out on silicone-coated release paper. A standard oven (Blue M Oven, Thermal Product Solutions, Pennsylvania, USA) was used to heat the films for dewetting. After dewetting, the resin was applied to the fiber bed by aligning and pressing constituents in an unheated hydraulic press (G30H-18-BCX, Wabash MPI).

3.2. Permeability

The effective transverse permeability was measured and compared for 8 plies of prepreg produced from the striped pattern, with 30% surface area exposed for each of the orientations, $[0/0]_n$, $[0/90]_n$, and $[0/90/\pm 45]_n$. These conditions were chosen to distinguish how sealed interfaces and tortuosity affected through-thickness air evacuation. The orientation $[0/0]_n$ represented the case of a large amount of sealed interfaces and a small tortuosity. On the other hand, $[0/90/\pm 45]_n$ represented the opposite case, where the amount of sealed interfaces was small and the tortuosity was large. Finally, $[0/90]_n$ represented the case where the proportions of sealed interfaces and the tortuosity were small. The values for sealed interfaces and tortuosity for these prepregs are summarized in Fig. 8a. Projected surface area exposed was not tested, since the results indicated that only ply count and single layer surface area exposed affected this parameter. Ply count was a specification that cannot be manipulated in a manufacturing setting, and a change in feature dimensions would invariably change values for the number of sealed interfaces and tortuosity.

In addition to samples created specifically for this study, samples from a previous report [11] were also included, thereby expanding the permeability data set to encompass other pattern types and feature dimensions. These samples included both a grid pattern and stacked in a $[0/90]_n$ orientation. The samples featured a single layer surface area exposed (%) of either 13% or 50%. The prepreg with an exposed surface area of 13% was likely to have a large number of sealed interfaces (~11%), as well as tortuous air evacuation pathways. The prepreg with an exposed surface area of 50% was likely to have no sealed interfaces (0%), and less tortuous air evacuation pathways.

A custom test fixture was used for the experiments [29], following the falling pressure method described by Tavares et al. [30] and Kratz et al. [29]. Plies of prepreg were laid over a cavity of known dimensions supported by stacks of honeycomb core. The edges of the plies were sealed with vacuum tape to prevent edge breathing, thus permitting air evacuation only in the through-thickness direction. The laminates were covered with perforated release film and breather cloth and were vacuum-bagged. Vacuum was drawn in the bag to compact the laminate and create a pressure difference between the core cavity and the bag. The evolution of pressure in the cavity was monitored over time using a pressure transducer and data acquisition software (LabVIEW, National Instruments), and the measurements were used to estimate an effective (slip-enhanced) permeability coefficient. All tests were performed at room temperature (~20 °C).

Tavares noted that gas flow in porous media generally enhances permeability through slippage of air molecules along the boundaries of the air-filled pores [31,32]. However, the Klinkenberg effect describes how slippage of gas along a pore wall gives rise to an apparent dependence of permeability on pressure [33]. This effect is applicable only when the Knudsen number (ratio of molecular mean free path length to a representative physical length scale) is between 0.01 and 0.1. Cender et al. [34] showed that at low resin saturation, the inter-tow pores of a prepreg contribute to higher permeability with no detectable Klinkenberg parameter. As resin saturation increases, inter-tow pores fill with resin, and gas can flow through the remaining unsaturated fiber tow, reducing the global prepreg permeability and producing a measurable Klinkenberg effect. In this work, the impregnation of resin into the fiber bed was virtually zero and the Klinkenberg effect was concluded to be negligible.

To obtain an average effective permeability value, two samples (replicates) were tested for each experimental configuration, with a minimum of three pressure decay trials per sample. Each trial was conducted to the time at which the cavity pressure stabilized (indicating flow had ceased), and the configuration was then re-pressurized to begin the next trial. The data from the first trial was omitted, because air evacuated more quickly when the consumables and plies had not been previously compacted.

Using Darcy's Law, the one-dimensional laminar flow of compressible air at isothermal and adiabatic conditions through a porous medium [29] can be described by

$$-\frac{KAP_{Bag}}{L\mu V_{Core}}t = ln\left[\frac{(P_{Core}(0)+P_{Bag})(P_{Core}(t)-P_{Bag})}{(P_{Core}(0)-P_{Bag})(P_{Core}(t)+P_{Bag})}\right] \quad (6)$$

where K is the permeability scalar in the flow direction in m^2, A is the cross-sectional area (1.46×10^{-2} m^2), P_{Bag} is the pressure at the bag side (5×10^3 Pa), P_{Core} is the pressure at the honeycomb core side in Pa, L is the lateral dimension in m, μ is the viscosity of air at room temperature (1.85×10^{-5} Pa*s), t is time in s, and V_{Core} is the volume of the core (7.87×10^{-4} m^3). Here, the vacuum level was assumed to be 95% (corresponding to an absolute vacuum bag pressure of 5 kPa). Plotting the left-hand side versus time yields a straight-line plot, the slope of which can be used to determine the effective air permeability of the prepreg, K.

(a)

Pattern Type	Single Layer A_{SE}	Orientation	Sealed Interfaces	Tortuosity
Stripes	30%	$[0/0]_n$	14.9% ± 12.7%	11.3 ± 4.4
		$[0/90]_n$	1.7% ± 4.7 %	9.1 ± 4.7
		$[0/90/\pm45]_n$	0.0% ± 0.0%	23.7 ± 11.6
Grid	13%	$[0/90]_n$	10.9% ± 8.4%	12.8 ± 5.7
	50%		0.0% ± 0.0%	2.9 ± 0.6

(b)

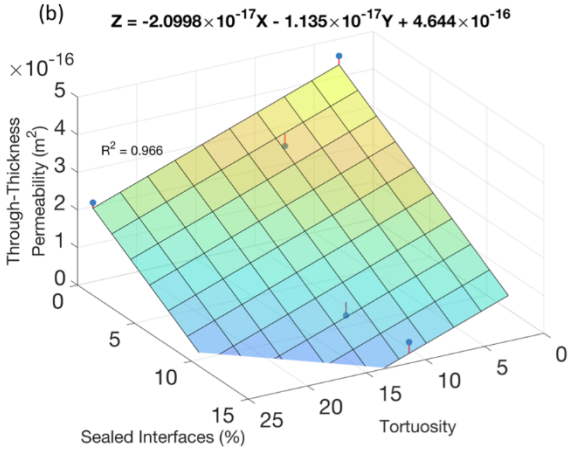

Fig. 8. (a) Summary of the sealed interfaces (%) and tortuosity values for each of the 8 ply prepreg samples studied for permeability. (b) Through-thickness permeability values (blue dots) of the tested prepregs and a planar fit (multi-colored plane) via a linear regression model with error bars indicated with red lines.

A summary of the permeability values of the laminates and a plane created by a linear regression fit of the data are presented in Fig. 8b. The equation for the linear regression model and the coefficient of determination (R^2) are also displayed in the graph. Sealed interfaces and tortuosity were defined by the variables X and Y, respectively. The value for R^2 (0.966) indicated that the model fit the data. The planar fit indicated that an increase in the percentage of sealed interfaces and in the tortuosity does indeed decrease the through-thickness permeability of the prepregs (a less desirable outcome for robust manufacturing). The equation indicated that the percentage of sealed interfaces had a larger effect on the decrease in permeability than did tortuosity.

3.3. Void content

Laminates were fabricated to determine parametric effects on internal porosity for each of the prototype prepregs evaluated in permeability tests. Laminates consisted of 8 plies of prepreg featuring a striped pattern of resin and 30% surface area exposed for each of the ply sequences, $[0/0]_n$, $[0/90]_n$, and $[0/90/\pm 45]_n$. Initially, each ply was cut to 150 × 150 mm, and trimmed to 140 × 140 mm after stacking. Standard vacuum bag procedures were used, except the edges were sealed using sealant tape to prevent in-plane air removal at the ply boundaries, thus allowing air evacuation only in the through-thickness direction. Sealed edges approximate commonly encountered process conditions that often restrict or prevent in-plane air evacuation – features such as large or complex parts and parts with ply drops or corners. A standard "ramp-hold" cure cycle was used.

Measurements of bulk void contents were performed using image analysis of polished sections prepared from each laminate center. Void contents were calculated from binary images processed to yield black and white pixels.

$$Porosity\ \ (\%) = \frac{p_{black}}{p_{white} + p_{black}} \times 100\% \tag{7}$$

where p is the number of pixels. Finally, an average internal porosity was determined from four images.

Laminates were fabricated using both 76 gsm and 152 gsm resin, and measured porosity levels are shown in Fig. 9a. The laminate with $[0/90]_n$ sequence featured no sealed interfaces and no tortuous air evacuation pathways, and yielded a void content of only ~0.1% (Fig. 9b). In contrast, the porosity levels in the $[0/0]_n$ and $[0/90/\pm 45]_n$ laminates were 1.0% (Fig. 9c) and 0.8% (Fig. 9d), respectively. The $[0/0]_n$ laminate represented the case of a large number of sealed interfaces, but relatively non-tortuous pathways for air evacuation, while the $[0/90/\pm 45]_n$ laminate represented the case of tortuous evacuation pathways and unsealed interfaces.

The experiments demonstrated that the prepreg and laminate features included in the study strongly influence the efficiency of gas evacuation during the cure cycle. The results also indicated specific aspects of prepreg design that most strongly affect this efficiency. In particular, sealed interfaces had a much greater effect on air permeability and void content after cure than tortuosity. The results and the methodology described here can be used to guide the design of discontinuous resin patterns for OoA prepregs.

4. Conclusions

This work outlined a methodology that allows for the rapid screening (i.e., evaluation and differentiation) of discontinuous resin patterns for VBO prepregs, which can be used to guide prepreg development. The methodology stems from previous work [11] that reported a technique to create discontinuous resin patterns of arbitrary shapes and sizes via a polymer film dewetting technique, which created a large design space for choosing a resin distribution. Due to the overwhelming number of choices in designing a prepreg with discontinuous resin format, selection of an appropriate resin distribution was not obvious. Thus, the methodology presented here allows one to differentiate between pattern types, feature dimensions, stacking orientations, and ply counts (with as many iterations as specified) without any physical experimentation by the use of simple geometric models. Experiments validate that the characteristics identified using the geometric model do indeed affect through-thickness air permeability and void content in cured laminates. In practice, the design space can be greatly reduced by eliminating patterns that do not allow for rapid air evacuation.

Various aspects of optimal design for prepregs with discontinuous resin distribution were outside the scope of this work, but would be important to pursue for future research. For example, the scope of this study did not include the changes in bulk factor due to feature dimensions and the subsequent effect on part quality. Smaller resin features with large surface openings will generally result in more efficient air evacuation, but the bulk factor will be much larger. A large bulk factor is associated with wrinkling in curved surfaces, which will

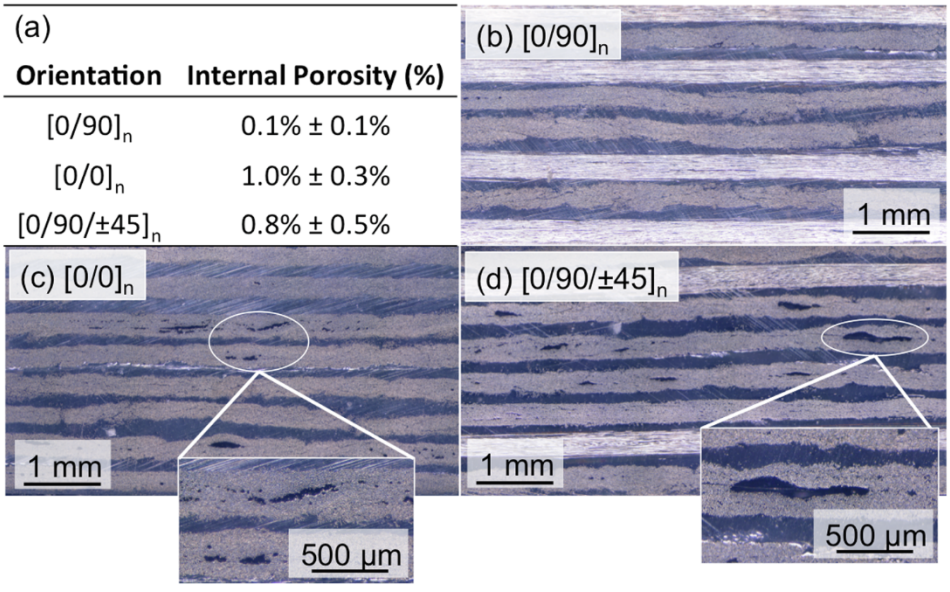

Fig. 9. (a) The measured internal porosity of each of the 8 ply prototype prepregs. (b–d) Cross-sections of the laminates made from each of the 8 ply prototype prepregs.

decrease the mechanical properties of the composite part. Secondly, the flow of resin during cure in relation to maximum feature dimensions was not evaluated. Full infiltration of a large surface opening requires longer flow distances and would be more challenging than small surface openings. Understanding the size restrictions on gap sizes with regard to resin flow would be useful to guide future prepreg designs for optimal resin distributions.

OoA/VBO prepreg processing presently suffers from a lack of robustness during manufacturing, often yielding unacceptable defect levels when manufacturing conditions are not fully controlled, are non-ideal, or complex part geometries are involved. The method described here provides a pathway to determine favorable (and, eventually, optimal) designs for prepregs with discontinuous resin distributions. Such prepregs can enable the manufacturing of composite parts with low defect levels without autoclaves, even in sub-optimal processing conditions. The robustness imparted by the methods presented can, in turn, expand the applicable uses of VBO prepregs within aerospace manufacturing and into other non-aerospace applications.

CRediT authorship contribution statement

Sarah G.K. Schechter: Conceptualization, Methodology, Software, Formal analysis, Investigation, Writing - original draft, Visualization. **Timotei Centea:** Conceptualization, Methodology, Writing - review & editing, Supervision. **Steven Nutt:** Writing - review & editing.

Acknowledgements

This project was supported by the M.C. Gill Composites Center. The authors are grateful for material donations from Airtech International (Cole Standish).

References

[1] Hahn GL, Bond GG, Fogarty JH. Non-Autoclave (Prepreg) Manufacturing Technology: Part Scale-Up with CYCOM 5320-1 Prepregs. In: Proc. SAMPE 2011 Conf., Long Beach, CA: 2011.
[2] Centea T, Grunenfelder LK, Nutt SR. A review of out-of-autoclave prepregs – material properties, process phenomena, and manufacturing considerations. Compos Part A Appl Sci Manuf 2015;70:132–54. https://doi.org/10.1016/j.compositesa.2014.09.029.
[3] Jackson K, Crabtree B. Autoclave quality composites tooling for composite from vacuum bag only processing. In: SAMPE Tech Conf, Long Beach, CA: 2002.
[4] Heth J. From art to science: a prepreg overview. High-Perform Compos 2000;8:32–6.
[5] Repecka L, Boyd J. Vacuum-bag-only-curable prepregs that produce void-free parts. In: SAMPE Tech Conf, Long Beach, CA: 2002.
[6] Centea T, Hubert P. Modelling the effect of material properties and process parameters on tow impregnation in out-of-autoclave prepregs. Compos Part A Appl Sci Manuf 2012;43:1505–13. https://doi.org/10.1016/j.compositesa.2012.03.028.
[7] Grunenfelder LK, Nutt SR. Void formation in composite prepregs - Effect of dissolved moisture. Compos Sci Technol 2010;70:2304–9. https://doi.org/10.1016/j.compscitech.2010.09.009.
[8] Roman M, Howard SJ, Boyd JD. Curable prepregs with surface openings. US 2014/0174641 A1, 2014.
[9] Grunenfelder LK, Dills A, Centea T, Nutt S. Effect of prepreg format on defect control in out-of-autoclave processing. Compos Part A Appl Sci Manuf 2017;93:88–99. https://doi.org/10.1016/j.compositesa.2016.10.027.
[10] Tavares SS, Michaud V, Månson JAE. Assessment of semi-impregnated fabrics in honeycomb sandwich structures. Compos Part A Appl Sci Manuf 2010;41:8–15. https://doi.org/10.1016/j.compositesa.2009.09.005.
[11] Schechter SGK, Centea T, Nutt SR. Polymer film dewetting for fabrication of out-of-autoclave prepreg with high through-thickness permeability. Compos Part A Appl Sci Manuf 2018;114:86–96. https://doi.org/10.1016/j.compositesa.2018.08.002.
[12] Kheshgi HS, Scriven LE. Dewetting: nucleation and growth of dry regions. Chem Eng Sci 1991;46:519–26. https://doi.org/10.1016/0009-2509(91)80012-N.
[13] Roy S, Bandyopadhyay D, Karim A, Mukherjee R. Interplay of substrate surface energy and nanoparticle concentration in suppressing polymer thin film dewetting. Macromolecules 2015;48:373–82. https://doi.org/10.1021/ma501262x.
[14] Coussy O. Surface Energy and Capillarity. Mech. Phys. Porous Solids. John Wiley & Sons, Ltd; 2010. p. 107–47.
[15] Kohl JG, Singer IL. Pull-off behavior of epoxy bonded to silicone duplex coatings. Prog Org Coatings 1999;36:15–20. https://doi.org/10.1016/S0300-9440(98)00074-5.
[16] Arafath ARA, Fernlund G, Poursartip A. Gas transport in prepregs: model and permeability experiments. In: Proc 17th Int Conf Compos Mater 2009:1–9.
[17] Helmus R, Centea T, Hubert P, Hinterhölzl R. Out-of-autoclave prepreg consolidation: coupled air evacuation and prepreg impregnation modeling. J Compos Mater 2016;50:1403–13. https://doi.org/10.1177/0021998315592005.
[18] Helmus R, Hinterhölzl R, Hubert P. A stochastic approach to model material variation determining tow impregnation in out-of-autoclave prepreg consolidation. Compos Part A Appl Sci Manuf 2015;77:293–300. https://doi.org/10.1016/j.compositesa.2015.03.021.
[19] Kourkoutsaki T, Comas-Cardona S, Binetruy C, Upadhyay RK, Hinterhoelzl R. The impact of air evacuation on the impregnation time of Out-of-Autoclave prepregs. Compos Part A Appl Sci Manuf 2015;79:30–42. https://doi.org/10.1016/j.compositesa.2015.08.034.
[20] Kompiš V, Qin QH, Fu ZJ, Chen CS, Droppa P, Kelemen M, et al. Parallel computational models for composites reinforced by CNT-fibres. Eng Anal Bound Elem 2012;36:47–52. https://doi.org/10.1016/j.enganabound.2011.04.009.
[21] Fahrang L, Fernlund G. Void evolution and gas transport during cure in out-of-autoclave prepreg laminates. In: Proc. SAMPE 2011 Conf.; 2011.
[22] Centea T, Hubert P. Measuring the impregnation of an out-of-autoclave prepreg by micro-CT. Compos Sci Technol 2011;71:593–9. https://doi.org/10.1016/j.compscitech.2010.12.009.
[23] Centea T, Hubert P. Out-of-autoclave prepreg consolidation under deficient pressure conditions. J Compos Mater 2014;48:2033–45. https://doi.org/10.1177/0021998313494101.
[24] Al-Raoush RI, Madhoun IT. TORT3D: A MATLAB code to compute geometric tortuosity from 3D images of unconsolidated porous media. Powder Technol 2017;320:99–107. https://doi.org/10.1016/j.powtec.2017.06.066.
[25] Allen TT. Introduction to engineering statistics and six sigma: Statistical quality control and design of experiments and systems. Springer Science & Business Media; 2006.
[26] Antony J. Design of Experiments for Engineers and Scientists. Elsevier; 2003.
[27] Saleh AKME, Arashi M, Tabatabaey SMM. Statistical Inference for Models with Multivariate t-Distributed Errors. New York: Wiley; 2014.
[28] Girden ER. Two-factor study with repeated measures on one factor. ANOVA 1992. https://doi.org/10.4135/9781412983419.
[29] Kratz J, Hubert P. Anisotropic air permeability in out-of-autoclave prepregs: Effect on honeycomb panel evacuation prior to cure. Compos Part A Appl Sci Manuf 2013;49:179–91. https://doi.org/10.1016/j.compositesa.2013.02.013.
[30] Tavares SS, Michaud V, Månson JAE. Through thickness air permeability of prepregs during cure. Compos Part A Appl Sci Manuf 2009;40:1587–96. https://doi.org/10.1016/j.compositesa.2009.07.004.
[31] Bear J. Dynamics of fluids in porous media. New York: American Elsevier Pub. Co.; 1972.
[32] Scheidegger AE. The physics of flow through porous media. Toronto: University of Toronto Press; 1958.
[33] Ho CK, Webb SW. Gas Transport in Porous Media. Springer Science & Business Media; 2006.
[34] Cender TA, Simacek P, Davis S, Advani SG. Gas evacuation from partially saturated woven fiber laminates. Transp Porous Media 2016;115:541–62. https://doi.org/10.1007/s11242-016-0784-x.